

Single-drop fragmentation determines size distribution of raindrops

Emmanuel Villermaux^{1,2*} and Benjamin Bossa¹

Like many natural objects, raindrops are distributed in size. By extension of what is known to occur inside the clouds, where small droplets grow by accretion of vapour and coalescence, raindrops in the falling rain at the ground level are believed to result from a complex mutual interaction with their neighbours. We show that the raindrops' polydispersity, generically represented according to Marshall–Palmer's law (1948), is quantitatively understood from the fragmentation products of non-interacting, isolated drops. Both the shape of the drops' size distribution, and its parameters are related from first principles to the dynamics of a single drop deforming as it falls in air, ultimately breaking into a dispersion of smaller fragments containing the whole spectrum of sizes observed in rain. The topological change from a big drop into smaller stable fragments—the raindrops—is accomplished within a timescale much shorter than the typical collision time between the drops.

The phenomenon of rain was first quantitatively documented in 1904 by Bentley¹ and von Lenard². While discussing his ingenious experiments (Fig. 1), Bentley noted: 'Perhaps the most remarkable fact, early brought to our notice, was the astonishing difference in the dimensions of the individual drops, both in the same and different rainfalls'. Indeed, subsequent measurements by Laws and Parsons³ and Marshall and Palmer⁴ showed that the raindrop size distribution is a monotonically decreasing function of the size: the number of drops $n(d)$ with size between d and $d + dd$ per unit volume of space is

$$n(d) = n_0 e^{-d/\langle d \rangle} \quad (1)$$

where n_0 is a constant reflecting the average spatial density of the drops, which depends on temperature⁵ and is equal to 0.08 cm^{-4} at the ground level, and $\langle d \rangle$ is an average diameter related to the rate of rainfall \mathcal{R} by

$$\langle d \rangle^{-1} = 41 \mathcal{R}^{-0.21} \quad (2)$$

where $\langle d \rangle$ is in centimetres and \mathcal{R} is in millimetres per hour. The distribution steepness is solely related to the intensity of rainfall: drop sizes are more broadly distributed in heavy storms than in fine mists. The observations suggesting the drop size repartition in equation (1), initially made from the record of drops' impacts on absorbing paper, were later cross-checked *in situ* by aircrafts flying through clouds and/or precipitation⁵, and by more refined measurements exploiting rain's radar echo reflectivity^{6,7}. If the interpretations of this law are diverse, its reality has now reached a consensus⁸.

Existing interpretations for rain initiation in the clouds rely on a sequence of nucleation plus condensation of ambient water vapour followed by coalescence of the colliding drops, possibly enhanced by turbulence (see refs 9, 10 and 11 for a review). Extension of these ideas to understand the drop size content of rain at the ground level^{6,12–16} emphasizes the (presumed) role of collision-induced break-up and coalescence between the drops in the falling rain. Precisely, if drop break-up is considered as an important partner in the overall process, it is only as a consequence of a collision

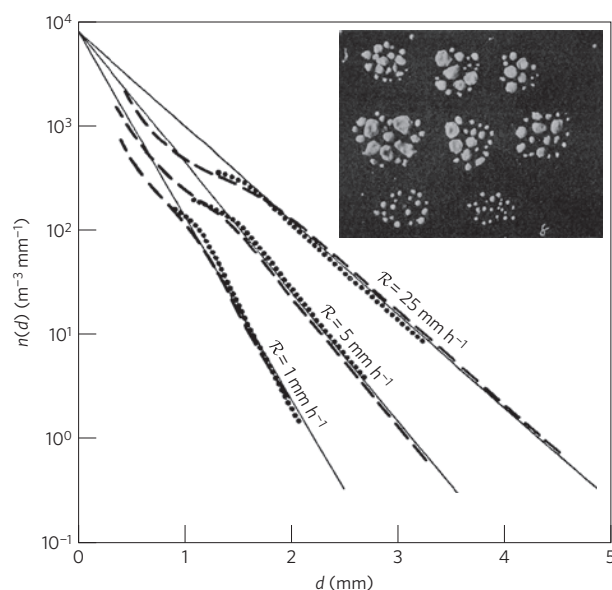


Figure 1 | Raindrops collected at the ground level, and their size distribution. Drop size histograms $n(d)$ for three different rainfall rates \mathcal{R} measured by Marshall and Palmer (adapted from their 1948 paper⁴). Inset: Raindrop specimens captured by Bentley (adapted from his 1904 paper¹) by allowing the drops to fall into a layer of fine uncompacted flour.

between drops, therefore emphasizing the prime importance of mutual interactions in the structure of rainfall⁸. Yet, the encounters between the drops have, in this vision, to be frequent enough for an equilibrium distribution to build through this mechanism, a fact, given the typical drop density in natural rain, that is unlikely^{13,17}.

The free-fall of a drop in a gaseous phase, its velocity², possible change of shape, inflation^{18–20}, destabilization^{21,22} and ultimate fragmentation^{12,23–26} have been studied in various contexts ranging from agricultural sewage, diesel engines, liquid propellant combustion and the physics of natural precipitation^{6,15,27}. Figure 2 shows how a liquid drop, falling in a counter-ascending air current

¹Aix-Marseille Université, IRPHE, 13384 Marseille Cedex 13, France, ²Institut Universitaire de France, 103 bd Saint Michel, 75005 Paris, France.

*e-mail: villermaux@irphe.univ-mrs.fr.

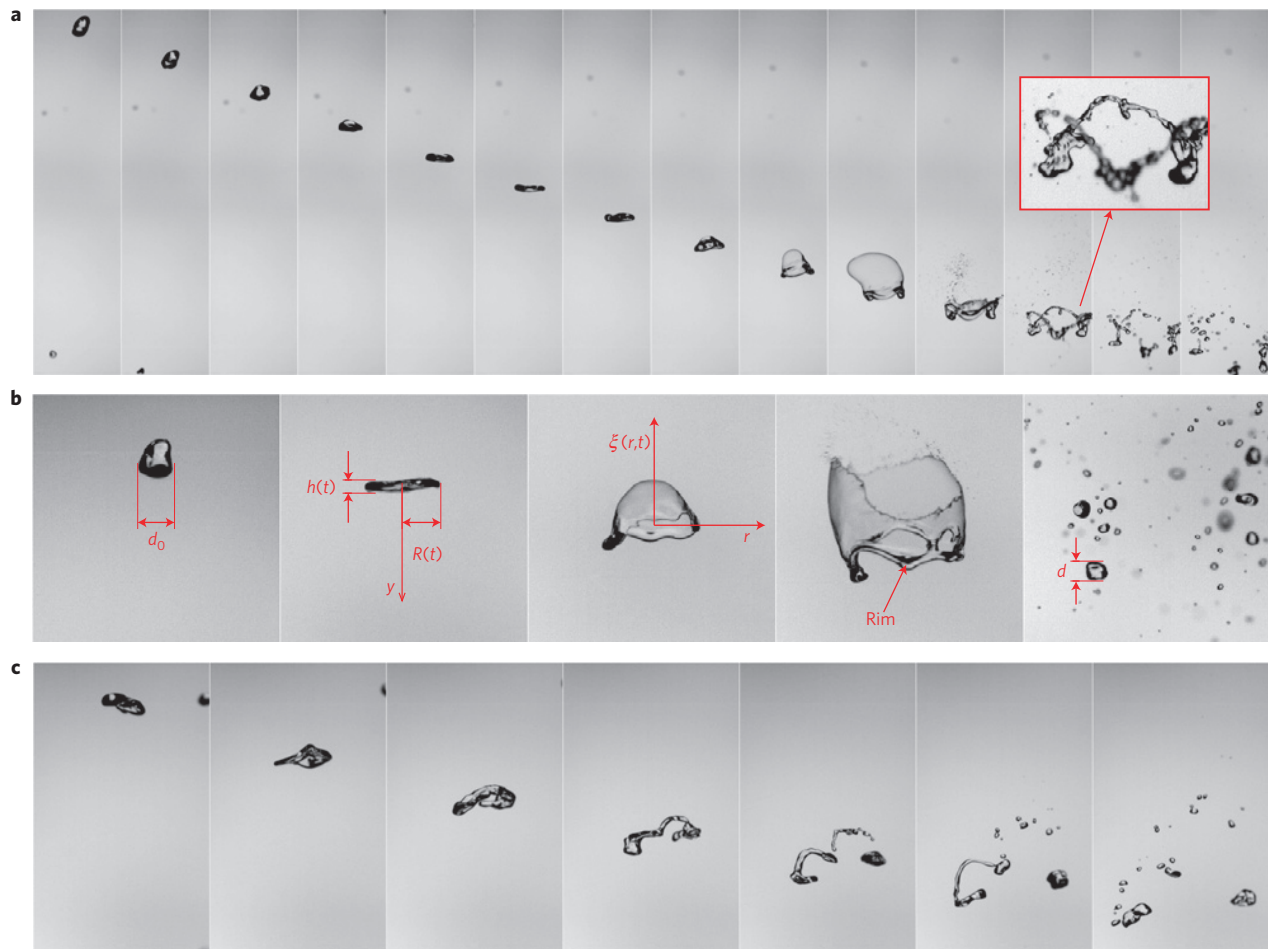


Figure 2 | Topological changes of falling drops and fragmentation. Top row: series of events of the fragmentation of a $d_0 = 6$ mm water drop falling in an ascending stream of air. The time interval between each image is $\Delta t = 4.7$ ms. The sequence shows first the flattening of the drop into a pancake shape, the inflation of a bag bordered by a thicker corrugated rim, its break-up and the destabilization of the rim itself (highlighted in the inset), leading to disjointed drops distributed in size. Middle row: a similar series defining the initial diameter d_0 , the bag thickness $h(t)$, its radius $R(t)$ and shape $\xi(r, t)$, and the final drop size d . Bottom row: the formation of a bag is not mandatory for the initial drop to break up. However, its fragmentation is always preceded by a change of topology into a ligament shape, which often occurs without bag inflation. The sequence is for $d_0 = 6$ mm and $\Delta t = 7.9$ ms.

generated by a big jet^{2,26} first deforms, then destabilizes and finally breaks into disjointed fragments that remain stable afterwards (see the movie of the overall sequence in the Supplementary Information), a phenomenon also known for liquid–liquid systems^{28,29}. The salient stages of this process, sometimes called ‘bag break-up’¹⁹ may be summarized as follows: (1) a change of topology of the initial drop, which flattens into a pancake shape as it decelerates downwards; (2) the formation of an inflating bag bordered by a toroidal rim collecting most of the initial drop volume and (3) a broad distribution of fragment sizes: the highly corrugated rim ultimately breaks into many small, and fewer larger drops.

We propose here a renewed vision of raindrop formation suggesting that both the functional form of equation (1), and the exponent and pre-factor of equation (2) are quantitatively understood from the fragmentation of a single drop²⁷. An original treatment of the drop dynamics shows moreover that its topological change into smaller fragments distributed according to equation (1) occurs when its size exceeds a critical value that we determine, and that it is accomplished within a timescale much shorter than the typical collision time between the drops in rain.

Rate of rainfall versus average drop size

The vertical altitude $z(t)$ of a liquid drop of volume $\Omega = \pi d_0^3/6$ and density ρ falling under gravity g in an ascending air stream of

density ρ_a and velocity V is ruled by

$$\frac{\ddot{z}}{g} = -1 + \frac{C_D}{2} \frac{\rho_a}{\rho} \frac{U^2}{g h} \quad (3)$$

where $U = -\dot{z} + V$ is the relative velocity between the drop and the air. As the drop falls, it deforms because of the stress (of order $\rho_a U^2$, a turbulent drag form that is suited to millimetre-sized drops at relative velocities of metres per second in air) at its surface, first into a rough pancake shape with radius $R(t)$ and thickness $h(t)$ such that $\Omega = \pi R^2 h$. The drag coefficient C_D is of order unity³⁰. Gravity and drag forces are eventually balanced, setting the equilibrium velocity of the drop. In the special case of rain for which $V = 0$, the velocity of a spherical drop $U = -\dot{z}(d_0) \sim \sqrt{(\rho/\rho_a) g d_0}$ is termed free-fall, or terminal velocity.

The quantitative link between the average drop size and the intensity of rain \mathcal{R} in equation (2) is readily made. The rate of fall \mathcal{R} expressed as a precipitation velocity (height of water collected at the ground per unit time) is

$$\mathcal{R} = \int n(d) (\pi d^3/6) U dd \quad (4)$$

where $U = \sqrt{(\rho/\rho_a) g d}$ is the free-fall velocity of a drop of size

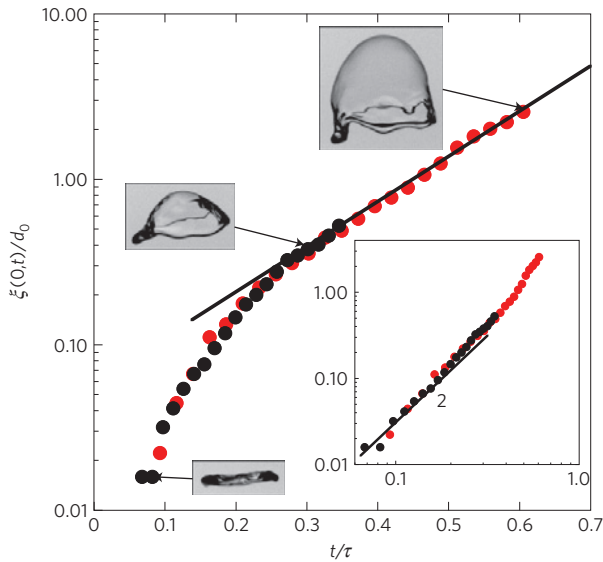


Figure 3 | Bag inflation. Temporal increase of the bag maximal amplitude $\xi(0, t)$ for two different initial drop sizes $d_0 = 6$ mm (red) and $d_0 = 12$ mm (black). The overall bag shape $\xi(r, t)$ is well represented around its maximum by the expected parabola in equation (11). The bag height first increases at constant acceleration ($\langle \xi \rangle / d_0 \sim 1/\tau^2$), and exponentially at later times, before bag break-up.

d. Let $P(d) = n(d) / \int n(d) dd$ be the drop size distribution, and $p(x) = \langle d \rangle P(d)$ with $x = d / \langle d \rangle$. Thus, $n(d) = n_0 p(x)$, leading to

$$\mathcal{R} = n_0 \frac{\pi}{6} \sqrt{\frac{\rho}{\rho_a}} \sqrt{g} \langle d \rangle^{\frac{2}{3}} \int x^{\frac{2}{3}} p(x) dx \quad (5)$$

that is

$$\langle d \rangle^{-1} \sim \mathcal{R}^{-\frac{3}{5}}$$

Up to a constant factor, equation (5) thus gives, from first principles, a precise estimate of the scaling exponent in equation (2) originally measured by Marshall and Palmer ($2/9 = 0.222\dots \approx 0.21$) and shows that it simply follows from the simple mass balance in equation (4). The pre-factor in equation (2) can be quantitatively estimated accordingly once the mechanism building the drop size distribution $P(d)$ is understood.

Drop topological change

The shape change of a spherical drop into an expanding pancake results from the stress repartition in the surrounding air at its surface. Let $\mathbf{U} = (U_r, U_y)$ be the axisymmetric velocity field in the vicinity of the drop, with y being a distance from its surface on the front side in the z direction and r a direction pointing radially (Fig. 2). The flow has locally the structure of a stagnation point $U_y = -\gamma y$, with a stretching rate γ set by the relative velocity U and the drop radius as $\gamma = U / (d_0/4)$. This stretching rate interpolates^{30,31} between that for a sphere ($U / (d_0/6)$) and for a disc ($U / (\pi d_0/4)$) of radius $d_0/2$. Thus, because

$$\rho_a U_r \partial_r U_r = -\partial_r p_a \quad \text{and} \quad \rho_a U_y \partial_y U_y = -\partial_y p_a$$

$$r \partial_r U_y + \partial_r (r U_r) = 0$$

for this inviscid, incompressible flow in the quasi-steady approximation, $p_a(r) = p(0) - \rho_a \gamma^2 r^2 / 8$ in the air, where $p(0) = \rho_a U^2 / 2$ is the stagnation pressure in $r = y = 0$. The pressure in the liquid is

equal to that in the air at the drop surface plus, according to Laplace law, a jump proportional to the drop surface curvature κ and to the liquid surface tension σ as $p(r) = p_a(r) + \sigma \kappa$. For $r \ll R(t)$, the drop is close to flat, so that the curvature term is weak and can be neglected, giving $p(r) \approx p(0) - \rho_a \gamma^2 r^2 / 8$. At the pancake border in $r = R(t)$ on the other hand, the interface radius of curvature is essentially half of the thickness $h(t)$; the curvature $\kappa \approx 2/h(t)$ is comparatively strong there, so that $p(R) = p(0) - \rho_a \gamma^2 R^2 / 8 + 2\sigma / h$. Thus, solving the axisymmetric Euler equation for the radial motion $u(r, t)$ inside the liquid drop

$$\rho (\partial_t u + u \partial_r u) = -\partial_r p \quad (6)$$

$$r \partial_t h + \partial_r (r u h) = 0 \quad (7)$$

with a time-dependent thickness $h(t)$, so that $u(r, t) = (r/R) \dot{R}$ owing to equation (7), gives, integrating equation (6) between $r = 0$ and $r = R(t)$,

$$\frac{1}{2} R \ddot{R} = -\frac{1}{\rho} \{p(R) - p(0)\}$$

Accounting for the pressure difference between the centre of the drop and its rim gives

$$\frac{\ddot{R}}{R} = \frac{1}{\tau^2} \left(1 - \frac{6}{We}\right) \quad (8)$$

where

$$\tau = \frac{d_0}{2U} \sqrt{\frac{\rho}{\rho_a}} \quad \text{and} \quad We = \frac{\rho_a U^2 d_0}{\sigma}$$

Viscous corrections can be incorporated in equation (6), but are superfluous for a low-viscosity liquid such as water and millimetre-sited drops.

As long as the Weber number We is moderate enough so that $We < 6$, the drop radius oscillates around a mean, with a frequency proportional to τ^{-1} . However, when $We > 6$, the radius $R(t)$ increases exponentially, initiating the burst of the drop on a timescale

$$\tau_{\text{burst}} \sim \frac{\tau}{\sqrt{1 - 6/We}} \quad (9)$$

proportional to the same timescale τ familiar in the atomization context²²: when $We \gg 6$, $\tau_{\text{burst}} \approx \tau$ and bursting has occurred by the time it takes for the drop to accelerate to reach the free-fall velocity $U/g \sim \sqrt{(\rho/\rho_a) d_0/g}$ (see equation (3)). The critical value $We = 6$ is consistent with ours and earlier observations^{21,32} when viscous corrections can be disregarded^{19,20}, as is the case for natural rain. From equation (7), it can be seen that the pancake thickness $h(t)$ obeys

$$\partial_t h + r \partial_r h + 2h = 0 \quad \text{with} \quad \tilde{t} = t \dot{R}/R$$

for which the asymptotic solution is an exponential decrease³³ of $h(t)$ independent of r as

$$h(t) \sim d_0 e^{-2\tilde{t}/\tau} \quad (10)$$

The momentum balance in the vertical direction solves the shape of the bag inflating concomitantly. Letting $\xi(r, t)$ be the vertical position of the bag, and assuming that $p(r)$ is a good estimate for

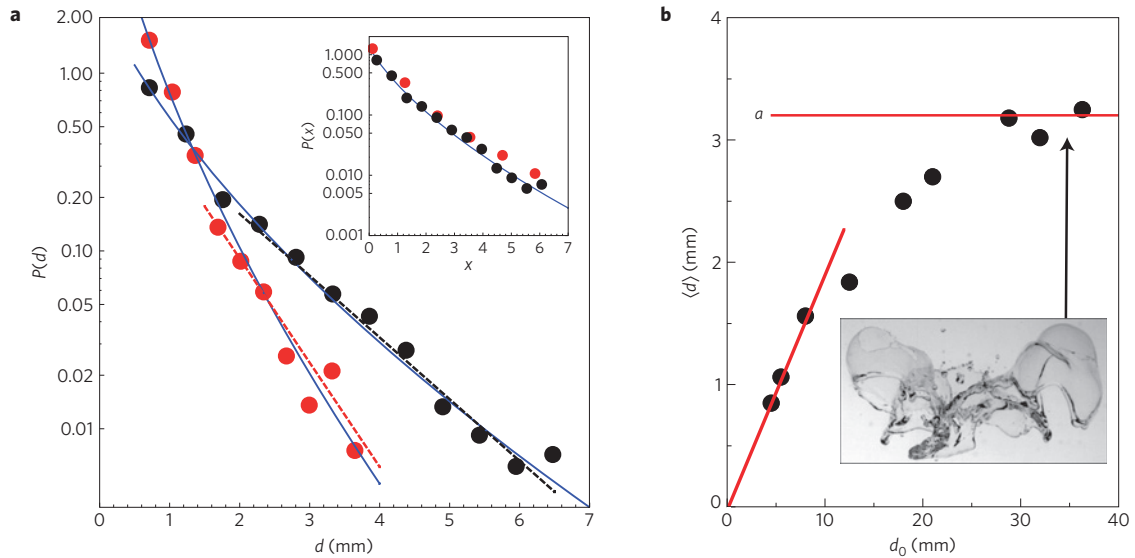


Figure 4 | Distribution of single-drop fragments. **a**, Distribution $P(d)$ of fragment sizes d for two initial diameters $d_0 = 6$ mm (red) and $d_0 = 12$ mm (black). The dashed lines are the Marshall-Palmer exponential distributions $P(d) = e^{-d/\langle d \rangle} / \langle d \rangle$ parametrized by the corresponding average diameters $\langle d \rangle$. The blue lines are the distribution function in equation (13). Inset: The distributions $p(x)$ of the scaled sizes $x = d/\langle d \rangle$ compared to the expected distribution in equation (13). **b**, The final average diameter $\langle d \rangle$ of the fragments versus the initial drop diameter d_0 . The relationship is proportional for small diameters, and saturates towards $\langle d \rangle \approx a = \sqrt{\sigma/\rho g}$.

the pressure difference between both sides of the bag^{30,34,35}, gives, in the slender slope approximation ($|\partial_r \xi(r, t)| \ll 1$),

$$\ddot{\xi}(r, t) = \frac{p(r)}{\rho h(t)}$$

Thus, using equation (10), when $\dot{\xi}(r, t=0) = 0$, gives

$$\xi(r, t) = \frac{p(r)}{\rho d_0} \frac{\tau^2}{4} (e^{2t/\tau} - 2t/\tau - 1) \quad (11)$$

that is, because $p(r)$ is quadratic in r , a parabola, for which the amplitude increases exponentially in time and the short-time ($t \ll \tau$) behaviour³⁵ is $\xi(r, t) \sim p(r)/(\rho d_0) t^2/2$, as shown in Fig. 3.

The overall drop–bag transition is accomplished within a time given by τ , and the bag thickness is uniform (a fact further confirmed by the constancy of the opening velocity of the hole when the bag breaks) and decays exponentially in time; there is no finite-time singularity in the case where the stress deforming the interface is applied normally as opposed to other cases where it is tangential³³. The reason why the bag ultimately breaks is that it is accelerated perpendicular to its surface, and may thus destabilize because of thickness modulations due to a Rayleigh–Taylor instability peculiar to thin films³⁶. The initial acceleration of the inflating bag for a given large We is $\ddot{\xi}(r, t) \sim d_0/\tau^2 \sim \sigma/(\rho d_0^2) = g(a/d_0)^2$, where $a = \sqrt{\sigma/\rho g}$ is the capillary length, of the order of 3 mm for water. The whole force per unit mass exerted on the drop is equal to g at terminal velocity (see equation (1)) and thus exceeds that due to the inflating motion for $d_0 > a$. The corresponding cutoff wavenumber k_c of the inflating pancake instability is equal to the capillary wavenumber constructed with the relevant acceleration³⁶. Thus, $k_c \sim 1/d_0$ for $d_0 < a$ and $k_c \sim 1/a$ for $d_0 > a$. This is why drops with a diameter that is initially a few units of a inflate as a whole, whereas larger drops deform into a collection of adjacent bags (Fig. 4 and ref. 37) of size given by a . As the bag inflates, thickness modulations grow (although at a slow rate, the growth rate of the instability shrinks according to $\sqrt{g k_c^2 h}$, where $k_c h \ll 1$) and finally break the film. At that moment, the drop essentially amounts to its toroidal rim, most

of the time very corrugated, which breaks by a capillary instability, forming drops. However large d_0 may be, the fragments' average size cannot exceed the capillary length a (Fig. 4 and ref. 38). The maximal size d_{\max} of a stable drop at terminal velocity in quiescent air for which both $U = \sqrt{(\rho/\rho_a) g d_{\max}}$ and $We = 6$ is

$$d_{\max} = a\sqrt{6} \quad (12)$$

giving $d_{\max} \approx 6$ mm, a value that indeed coincides with the cutoff sizes recorded in natural rain (Fig. 1 and ref. 4).

Drop size distribution

Corrugated rims, whether they come from the drop–pancake–bag transition described above or from a direct topology change from a drop to a ligament (Fig. 2) due to random motions of the air, build the overall drop size distribution in the resulting spray. Consider a collection of ligaments, all of them with a given volume $\Omega = \pi d_1^3/6$, breaking as they are strongly corrugated. Strong corrugation means that the amplitude of the cross-section diameter fluctuations along the ligament is of the order of its mean radius. The break-up of these ligaments is known²⁷ to produce drop size distributions well represented by Gamma distributions $\Gamma_n(x = d/d_1) = n^n x^{n-1} e^{-nx} / \Gamma(n)$ of order $n = 4$ and average d_1 . The big drops in this distribution have a relative fraction decaying exponentially according to $e^{-n d/d_1}$. These big drops are likely to suffer subsequent break-up and crossover the critical condition $We = 6$ after the first break-up, and do so as long as they all remain stable. The overall drop size distribution in rain is thus a compound³⁹ of stable drops coming from the break-up of drops essentially exponentially distributed in size as

$$P(d) = \int \Gamma_4(d, d_1) \frac{e^{-d_1/(d)}}{\langle d \rangle} dd_1$$

providing

$$p(x = d/\langle d \rangle) = \frac{32}{3} x^{\frac{3}{2}} K_3(4\sqrt{x}) \quad (13)$$

$$\approx e^{-x} \quad \text{for } x \gtrsim \mathcal{O}(1)$$

where $K_3(\cdot)$ is the Bessel function of order 3. This distribution has the qualitative shape of the fragment distributions recorded in several related situations^{12,23–26,40}, and fits precisely our experiments (Fig. 4). This distribution is also consistent with Marshall–Palmer’s law: its wing above the mean is exponential, with an argument set by the overall average drop size. This broad distribution is solely parametrized by the average diameter $\langle d \rangle$ or, alternatively, by a given rate of rainfall \mathcal{R} (see equations (2) and (5)). Natural rain is known to be ‘patchy’^{34,42}, with associated temporal and spatial fluctuations of \mathcal{R} . These fluctuations may affect $P(d)$, but cannot be solely responsible for its shape^{17,42}. If that were the case, the fluctuations in \mathcal{R} should be such that they screen the dispersion of drop sizes produced by a single break-up event; however, that dispersion already contains the whole spectrum of observed sizes, at constant \mathcal{R} (ref. 40).

The complete relationship in equation (5) can now be computed. Using $n_0 = 0.08 \text{ cm}^{-4}$, $\rho/\rho_a = 10^3/1.2$, $g = 9.81 \text{ m s}^{-2}$ and $\int_0^\infty x^{7/2} p(x) dx \approx 28.3$ with $p(x)$ given by equation (13) yields

$$\langle d \rangle^{-1} = 48.5 \mathcal{R}^{-\frac{2}{9}}$$

in the units of equation (2) giving, in addition to the exponent, a good order of magnitude for the pre-factor between the steepness of the drop size distribution and the rate of fall.

Timescales

In the above scenario, the complete distribution $P(d)$ is constructed from big liquid lumps released intermittently at the base of the clouds within a time given by equations (9) and (12) $\tau_{\text{burst}} \sim \tau/\sqrt{1-(d_{\text{max}}/d_0)^2}$, regardless of any interaction between nearby drops in the falling rain. The corresponding bursting distance $Z_{\text{burst}} = U \tau_{\text{burst}}$ is given by

$$\frac{Z_{\text{burst}}}{d_0 \sqrt{\rho/\rho_a}} = \frac{1}{\sqrt{1-(d_{\text{max}}/d_0)^2}}$$

and is of the order of a few tens of initial drop diameters $Z_{\text{burst}} = d_0 \sqrt{\rho/\rho_a}$ for large drops with $d_0 \gg d_{\text{max}}$, that is, not far from the cloud’s base, where Marshall–Palmer distributions have indeed been observed^{43,44}, and diverges when $d_0 \rightarrow d_{\text{max}} \approx 6 \text{ mm}$. There is a critical slowing down of the drop’s shape dynamics when d_0 approaches d_{max} (refs 12, 40). The fact that this vision provides precise and quantitative predictions is not a coincidence because collisions between independent drops in the process of breaking are less frequent than their individual bursting frequency. Consider for instance rain with a water content corresponding to an average drop size $\langle d \rangle$ at the ground level, with a volume of water $n_0 \langle d \rangle^4$ per unit volume of space. This volume was initially confined into $N(d_0)$ big drops of diameter d_0 , per unit volume of space, distant from each other by the mean free path $1/N(d_0) d_0^2 = d_0/n_0 \langle d \rangle^4$. A lower bound for the collision time τ_{coll} is the time it takes to travel at the free-fall velocity U between two drops separated by the mean free path. Comparing this with the bursting time τ_{burst} above gives

$$\frac{\tau_{\text{burst}}}{\tau_{\text{coll}}} = \frac{n_0 \langle d \rangle^4 \sqrt{\rho/\rho_a}}{\sqrt{1-(d_{\text{max}}/d_0)^2}} \approx 2 \times 10^{-2}$$

with $\langle d \rangle \approx 0.3 \text{ cm}$ and $d_0 \gg d_{\text{max}}$. The corresponding bursting time $\tau_{\text{burst}} \approx \tau \approx 10^{-2} \text{ s}$ is also much smaller than the falling time of a typical drop from the clouds a kilometre away from the ground; this solves the paradox inherent to the vision where coalescence is thought to be the main ingredient building the distribution, although the number of collisions is not large enough for a stable distribution to emerge^{13,17}.

The conclusion is opposite in the clouds. There, the droplet density is typically much higher (about 10^2 cm^{-3}), but especially their average diameter $\langle d \rangle \approx 10^{-3} \text{ cm}$ is much smaller¹⁵, so that they do not break up ($We < 6$, see equation (8)). Drops thus do have time to coalesce ballistically, and even more efficiently when turbulence-induced aggregation mechanisms are accounted for^{10,11}, to grow in size. They ultimately fall when they are heavy enough to overcome the buoyant ascending motions at the base of the cloud, and then burst, setting the size repartition in the rain that wets the ground.

A challenging investigation would be to visualize the above scenario *in situ* in precipitation, in real time as in Fig. 2 to check the relevance of the timescale τ and critical condition for bursting $We = 6$ in real rain, and compare the measured instantaneous and global statistics of $P(d)$. An interesting extension would also be to consider the same fragmentation problem with, instead of liquid drops confined by surface tension, brittle solids with a weak tenacity (critical stress), such as snowflakes, for which the size distribution is ruled by the same type of law as in equation (1) (refs 5, 44, 45).

Received 5 November 2008; accepted 17 June 2009; published online 20 July 2009

References

- Bentley, W. Studies of raindrops and raindrop phenomena. *Mon. Weath. Rev.* **10**, 450–456 (1904).
- von Lenard, P. Über regen. *Meteorol. Z.* **06**, 92–262 (1904).
- Laws, J. & Parsons, D. The relation of raindrop-size to intensity, ii. *Trans. Am. Geophys. Union* **24**, 452–460 (1943).
- Marshall, J. S. & Palmer, W. M. The distribution of raindrops with size. *J. Meteorol.* **5**, 165–166 (1948).
- Houze, R. A., Hobbs, P. V. & Herzegh, P. H. Size distributions of precipitation particles in frontal clouds. *J. Atmos. Sci.* **36**, 156–162 (1979).
- Mason, B. J. *The Physics of Clouds* (Clarendon, 1971).
- Ulbrich, W. C. A review of the differential reflectivity technique of measuring rainfall. *IEEE Trans. Geosci. Remote Sensing* **GE-24**, 955–965 (1986).
- Testik, F. Y. & Barros, A. P. Towards elucidating the microstructure of warm rainfall: A survey. *Rev. Geophys.* **45**, 1–21 (2007).
- Langmuir, I. The production of rain by a chain reaction in cumulus clouds at temperature above freezing. *J. Meteorol.* **5**, 175–192 (1948).
- Falkovich, G., Fouxon, A. & Stepanov, M. Acceleration of rain initiation by turbulence. *Nature* **419**, 151–154 (2002).
- Pruppacher, H. R. & Klett, J. D. *Microphysics of Clouds and Precipitation* (Kluwer–Academic, 1997).
- Kombayasi, M., Gonda, T. & Isono, K. Life time of water drops before breaking and size distribution of fragment droplets. *J. Met. Soc. Japan* **42**, 330–340 (1964).
- Srivastava, R. Size distribution of raindrops generated by their breakup and coalescence. *J. Atmos. Sci.* **28**, 410–415 (1971).
- Low, T. & List, R. Collision, coalescence and breakup of raindrops. Part i: Experimentally established coalescence efficiencies and fragment size distributions in breakup. *J. Atmos. Sci.* **39**, 1591–1606 (1982).
- Seinfeld, J. H. & Pandis, S. N. *Atmospheric Chemistry and Physics* (Wiley, 1998).
- Barros, A. P., Prat, O. P., Shrestha, P., Testik, F. Y. & Bliven, L. F. Revisiting Low and List (1982): Evaluation of raindrop collision parametrizations using laboratory observations and modeling. *J. Atmos. Sci.* **65**, 2983–2993 (2008).
- Kostinski, A. B. & Jameson, A. Fluctuation properties of precipitation. Part iii. On the ubiquity and emergence of the exponential drop size spectra. *J. Atmos. Sci.* **56**, 111–121 (1999).
- Lane, W. Shatter of drops in streams of air. *Ind. Eng. Chem.* **43**, 1312–1317 (1951).
- Pilch, M. & Erdman, C. Use of breakup time data and velocity history data to predict the maximum size of stable fragments for acceleration-induced breakup of a liquid drop. *Int. J. Multiphase Flow* **13**, 741–757 (1987).
- Chou, W.-H. & Faeth, G. M. Temporal properties of secondary drop breakup in the bag breakup regime. *Int. J. Multiphase Flow* **24**, 889–912 (1998).
- Hanson, A. R., Domich, E. G. & Adams, H. S. Shock tube investigation of the break-up of drops by air blasts. *Phys. Fluids* **6**, 1070–1080 (1963).
- Ranger, A. A. & Nicholls, A. J. Aerodynamic shattering of liquid drops. *AIAA J.* **7**, 285–290 (1969).
- Fournier d’Albe, E. M. & Hidayetulla, S. M. The break-up of large water drops falling at terminal velocity in free air. *Q. J. R. Meteorol. Soc.* **81**, 610–613 (1955).
- Magarvey, H. R. & Taylor, W. B. Free fall breakup of large drops. *J. Appl. Phys.* **27**, 1129–1135 (1956).

25. Magarvey, H. R. & Taylor, W. B. Shattering of large drops. *Nature* **177**, 745–746 (1956).
26. Alusa, A. L. & Blanchard, D. C. Drop size distribution produced by the breakup of large drops under turbulence. *J. Recherches Atmos.* **VII**, 1–9 (1971).
27. Villermaux, E. Fragmentation. *Annu. Rev. Fluid Mech.* **39**, 419–446 (2007).
28. Thomson, J. J. & Newall, M. A. On the formation of vortex rings by drops. *Proc. R. Soc. London* **39**, 417–436 (1885).
29. Buah-Bassuah, P. K., Rojas, R., Residori, S. & Arecchi, F. T. Fragmentation instability of a liquid drop falling inside a heavier miscible fluid. *Phys. Rev. E* **72**, 067301 (2005).
30. Batchelor, G. K. *An Introduction to Fluid Dynamics* (Cambridge Univ. Press, 1967).
31. Lamb, H. *Hydrodynamics* 6th edn (Cambridge Univ. Press, 1932).
32. Hinze, J. O. Fundamentals of the hydrodynamic mechanism of splitting in dispersion processes. *AIChE J.* **1**, 289–295 (1949).
33. Paruchuri, S. & Brenner, M. P. Splitting of a jet. *Phys. Rev. Lett.* **98**, 134502 (2007).
34. Taylor, G. I. The shape and acceleration of a drop in a high speed air stream. *Collected Papers III*, 457–464 (1949).
35. Engel, O. G. Fragmentation of water drops in the zone behind an air shock. *J. Res. Nat. Bur. Stand.* **60**, 245–280 (1958).
36. Bremond, N. & Villermaux, E. Bursting thin liquid films. *J. Fluid Mech.* **524**, 121–130 (2005).
37. Reyssat, E., Chevy, F., Biance, A. L., Petitjean, L. & Quéré, D. Shape and instability of free-falling liquid globules. *Europhys. Lett.* **34005** (2007).
38. Matthews, B. J. & Mason, J. B. Electrification produced by the rupture of large water drops in an electric field. *Q. J. R. Meteorol. Soc.* **90**, 275–286 (1964).
39. Ulbrich, W. C. Natural variations in the analytical form of the raindrop size distribution. *J. Clim. Appl. Meteorol.* **22**, 1764–1775 (1983).
40. Blanchard, D. C. & Spencer, A. T. Experiments on the generation of raindrop-size distributions by drop breakup. *J. Atmos. Sci.* **27**, 101–108 (1970).
41. Liu, Y. Statistical theory of the Marshall-Palmer distribution of raindrops. *Atmos. Eng.* **27A**, 15–19 (1993).
42. Jameson, A. R. & Kostinski, A. A. What is a raindrop size distribution? *Bull. Am. Meteorol. Soc.* **82**, 1169 (2001).
43. Blanchard, D. C. Raindrop size distribution in Hawaiian rains. *J. Meteorol.* **10**, 457–473 (1953).
44. Ohtake, T. Observations of size distributions of hydrometers through the melting layer. *J. Atmos. Sci.* **26**, 545–557 (1969).
45. Gunn, K. L. S. & Marshall, J. S. The distribution with size of aggregate snowflakes. *J. Meteorol.* **15**, 452–461 (1958).

Acknowledgements

This work has been supported by the Office National d'Études et Recherches Aéropatiales (ONERA) under contract F/20215/DAT-PPUJ and Agence Nationale de la Recherche (ANR) through grant ANR-05-BLAN-0222-01.

Author contributions

E.V. designed and carried out the experiments, analysed the data and wrote the paper; B.B. helped in the experiments and image processing.

Additional information

Supplementary information accompanies this paper on www.nature.com/naturephysics. Reprints and permissions information is available online at <http://npg.nature.com/reprintsandpermissions>. Correspondence and requests for materials should be addressed to E.V.